Journal of Systems Engineering and Electronics
Vol. 33, No. 1, February 2022, pp.188 – 196

Robust adaptive control of hypersonic vehicle considering inlet unstart

WANG Fan [1], FAN Pengfei [1,*], FAN Yonghua [1], XU Bin [2], and YAN Jie [1]

1. College of Astronautics, Northwestern Polytechnical University, Xi'an 710072, China;
2. College of Automation, Northwestern Polytechnical University, Xi'an 710072, China

Abstract: In this paper, a model reference adaptive control (MRAC) augmentation method of a linear controller is proposed for air-breathing hypersonic vehicle (AHV) during inlet unstart. With the development of hypersonic flight technology, hypersonic vehicles have been gradually moving to the stage of weaponization. During the maneuvers, changes of attitude, Mach number and the back pressure can cause the inlet unstart phenomenon of scramjet. Inlet unstart causes significant changes in the aerodynamics of AHV, which may lead to deterioration of the tracking performance or instability of the control system. Therefore, we firstly establish the model of hypersonic vehicle considering inlet unstart, in which the changes of aerodynamics caused by inlet unstart is described as nonlinear uncertainty. Then, an MRAC augmentation method of a linear controller is proposed and the radial basis function (RBF) neural network is used to schedule the adaptive parameters of MRAC. Furthermore, the Lyapunov function is constructed to prove the stability of the proposed method. Finally, numerical simulations show that compared with the linear control method, the proposed method can stabilize the attitude of the hypersonic vehicle more quickly after the inlet unstart, which provides favorable conditions for inlet restart, thus verifying the effectiveness of the augmentation method proposed in the paper.

Keywords: air-breathing hypersonic vehicle (AHV), inlet unstart, model reference adaptive control augmentation (MRAC), radial basis function (RBF) neural network.

DOI: 10.23919/JSEE.2022.000019

1. Introduction

With the development of air-breathing hypersonic vehicles (AHVs), key technologies such as scramjet technology, airframe-propulsion integration technology, thermal protection technology, and flight control technology have made great progress, and all military powers have moved forward from flight test to engineering application. As a kind of weapons, air breathing hypersonic vehicle need to maneuver according to the guidance law. During maneuvers, low Mach number, large angle of attack, and high back pressure of the isolator may cause the terminal normal shock wave to be pushed out of the inlet, resulting in the inlet unstart. As a result, the internal and external flow field of the vehicle will be changed due to inlet unstart, and the AHV will experience an instantaneous loss of thrust and a sudden change in aerodynamic characteristics. Consequently, the tracking performance of flight control system deteriorates and even the flight control system impulsively transforms into unstable flight conditions [1]. The flight test jointly conducted by Defence Advanced Research Projects Agency and Queensland University of Australia in 2007 and the x-51A flight test in 2010 and 2011 failed due to the unstart of scramjet inlet [2−4]. The unstart of the inlet of the scramjet engine has attracted wide attention from researchers. Im et al. [5] examined recent research progress in identifying flow choking mechanisms that trigger unstart and discussed three different flow choking mechanisms. Kong et al. [6] detected inlet unstart by estimating the location of the shock train leading edge based on the flowfield reconstruction model, and the detection accuracy was greatly improved. Devaraj et al. [7] performed experiments in the hypersonic wind tunnel of Indian Institute of Science at Mach 6 to study unstart characteristics of generic scramjet intakes. Xue et al. [8] proposed a few novel data-analyzed methods based on the analysis of the schlieren images and dynamic pressure to study the dynamic characteristics of separation shock in an unstarted hypersonic inlet flow. Li et al. [9] analyzed flow characteristics during the start/unstart transition and discussed the influences of the backpressure and transition stage on the hysteresis behavior of the transition in detail. Deng et al. [10] investigated unstart process of dual-mode scramjet from a started state to an unstarted state numerically at the free-stream Mach number of 4 and predicted unstart phe-

Manuscript received August 12, 2019.
*Corresponding author.
This work was supported by the Foundation of Shanghai Aerospace Science and Technology (SAST2016077).

nomenon by applying time histories of static pressure and mass flow rate. Bolender et al. [11] observed slope reversal in stability and control derivatives during unstart, and found that the unstarted inlet destabilized the controller designed using the started inlet aerodynamics. In summary, current research on inlet unstart problem mainly concentrates on its mechanism, detection, characteristics, hysteresis behavior, prediction and aerodynamic variation caused by inlet unstart. Whereas solving the problem of inlet unstart by flight control are investigated in the initial phase. In this paper, the attitude stability of the aircraft after the inlet unstart is realized by flight control, which creates conditions for the inlet restart.

Model reference adaptive control (MRAC) has been shown to successfully handle dynamical systems with parameter perturbations and external disturbances due to its strong robustness and adaptation. In [12], a classical open-loop reference model design and a modified closed-loop reference model design were applied to the road runner six-degree-of-freedom generic hypersonic vehicle model with uncertainty in control effectiveness, longitudinal center of gravity location, aerodynamic coefficients, sensor bias and noise, and input time delays. In [13], Lavretsky et al. designed and analyzed a predictor-based MRAC which yielded improved transient characteristics. In [14], a direct MRAC framework provided stable adaptation in the presence of multi-input constraints for a class of multi-input dynamical systems with unknown parameters and matched uncertainties. While one drawback of the MRAC is the large number of design parameters to be scheduled by trial and error. Therefore, some kind of automated and intelligent procedure to extricate the designer from the cumbersome and time-consuming work is needed.

Radial basis function (RBF) neural network can approximate any continuous function to any desired accuracy [15]. This characteristic of RBF neural network makes it widely used in the estimation and identification of system parameters. Combining RBF neural network with other control methods, a variety of novel control methods are proposed. Wang et al. [16] proposed sliding mode controller with radial basis function neural network (RBFNN) identifying uncertainty parameters, which removed the chattering and reserved the fast, robust, immunity of sliding mode control. Zhai et al. [17] designed the sliding mode fault tolerant controller with RBFNN estimating the unknown additive fault and adaptive method dealing with the partial loss of effectiveness fault. Slama et al. [18] presented an RBFNN MRAC system containing RBFNN models, RBFNN controllers, RBFNN reference models and an adjustment mechanism for multiple input multiple output nonlinear systems. Whereas there has been little research on using RBF to schedule adaptive parameters of MRAC.

In practical engineering application, the aircraft already has baseline controller including proportion and integral. In this paper, based on the baseline controller, the adaptive unit is added to augment the baseline controller, that is, the total control input is the sum of baseline linear control and adaptive control, which can not only restore the expected performance of the controller, but also make the least changes to the baseline controller. This method is convenient for engineering implementation and is significant to solve engineering problems. Therefore, an MRAC augmentation method of a linear controller is proposed for the longitudinal short-period dynamics of AHV to provide a stable attitude quickly after the inlet unstart.

In summary, the contributions of this paper are explained as follows:

(i) The model of hypersonic vehicle inlet unstart is established;

(ii) An MRAC augmentation method of a linear controller is proposed to solve the problem of attitude stabilization of hypersonic vehicle when inlet unstart;

(iii) RBF neural network is used to adjust the parameters of adaptive control quickly;

(iv) The simulation results show that the MRAC augmentation method of linear controller can stabilize the attitude of the aircraft more quickly when the inlet unstart, which creates favorable conditions for the restart of the inlet.

The paper is organized as follows: Section 2 describes the longitudinal model for a hypersonic vehicle with the start and unstart inlet. Section 3 proposes a MRAC augmentation method of linear controller. Section 4 presents simulation results. Finally, Section 5 gives conclusions.

2. Longitudinal model of a hypersonic vehicle

The longitudinal motion equations of the rigid hypersonic vehicle in the start regime are given as follows [19,20]:

$$\begin{cases} \dot{V} = \dfrac{T\cos\alpha - D}{m} - g\sin\gamma \\ \dot{\gamma} = \dfrac{T\sin\alpha + L}{mV} - \dfrac{g\cos\gamma}{V} \\ \dot{Q} = \dfrac{M_{yy}}{I_{yy}} \\ \dot{\vartheta} = Q \\ \dot{\alpha} = Q - \dfrac{T\sin\alpha + L}{mV} + \dfrac{g\cos\gamma}{V} \end{cases} \tag{1}$$

where V, γ, Q, ϑ, and α represent velocity, flight-path angle, pitch rate, pitch angle, and angle of attack, respectively. I_{yy} and m are moments of inertia and mass of the hypersonic vehicle respectively. g is the acceleration of gravity. M_{yy}, T, D, and L denote pitching moment,

thrust, drag, and lift, respectively. The approximations of force and moment are expressed as follows:

$$\begin{cases} M_{yy} = \bar{q}S\bar{c}C_{M_{yy}} \\ T = \bar{q}SC_T \\ D = \bar{q}SC_D \\ L = \bar{q}SC_L \end{cases} \tag{2}$$

where $C_{M_{yy}}$, C_T, C_D, and C_L present the coefficient of pitching moment, thrust, drag , and lift, respectively. S, $\bar{c}$, and $\bar{q}$ denote reference area, reference length, and dynamic pressure

$$\bar{q} = \frac{1}{2}\rho V^2 \tag{3}$$

where ρ denotes air density.

The coefficients of longitudinal force and moment are as follows [19]:

$$\begin{cases} C_{M_{yy}} \approx C_{Myy0} + C_{M_{yy}}^{\alpha}\alpha + C_{M_{yy}}^{\alpha^2}\alpha^2 + C_{M_{yy}}^{\delta_e}\delta_e \\ C_T \approx C_{T0} + C_T^{\alpha}\alpha + C_T^{\alpha^2}\alpha^2 + C_T^{\alpha^3}\alpha^3 \\ C_D \approx C_{D0} + C_D^{\alpha}\alpha + C_D^{\alpha^2}\alpha^2 + C_D^{\delta_e}\delta_e + C_D^{\delta_e{}^2}\delta_e{}^2 \\ C_L \approx C_{L0} + C_L^{\alpha}\alpha + C_L^{\delta_e}\delta_e \end{cases} \tag{4}$$

where δ_e is the elevator deflection angle.

The nonlinear equation of motion (1) is linearized with small perturbation method:

$$\begin{cases} \dot{\alpha} = -a_4\alpha + Q - a_5\delta_e \\ \dot{Q} = -a_2\alpha - a_1 Q - a_3\delta_e \end{cases} \tag{5}$$

where

$$a_1 = \frac{-C_{M_{yy}}^{Q}\bar{q}S\bar{c}}{J_{yy}},$$

$$a_2 = \frac{-C_{M_{yy}}^{\alpha}\bar{q}S\bar{c}}{J_{yy}},$$

$$a_3 = \frac{-C_{M_{yy}}^{\delta_e}\bar{q}S\bar{c}}{J_{yy}},$$

$$a_4 = \frac{(T + \bar{q}SC_L^{\alpha})}{mV},$$

$$a_5 = \frac{\bar{q}SC_L^{\delta_e}}{mV}.$$

The linearized dynamic equations (5) can be written in the form of the following state space:

$$\begin{cases} \dot{\boldsymbol{x}} = \boldsymbol{A}\boldsymbol{x} + \boldsymbol{B}\boldsymbol{u} \\ \boldsymbol{y} = \boldsymbol{C}\boldsymbol{x} \end{cases} \tag{6}$$

where the state vector $\boldsymbol{x} = [\alpha\ Q]^{\mathrm{T}}$, the control vector $\boldsymbol{u} = \delta_e$, the output vector $\boldsymbol{y} = \alpha$, and the coefficient matrices are as follows:

$$\boldsymbol{A} = \begin{bmatrix} -a_4 & 1 \\ -a_2 & -a_1 \end{bmatrix},\ \boldsymbol{B} = \begin{bmatrix} -a_5 \\ -a_3 \end{bmatrix},\ \boldsymbol{C} = [1 \quad 0].$$

During an un-start event, the shock system in the inlet moves forward and out of the inlet due to a downstream rise in stagnation pressure. The shock system moving out of the inlet results in a significant pressure rise on the inlet that is manifested as a positive slope in the moment as a function of angle-of-attack that either de-stabilizes a stable aircraft or makes an unstable aircraft more unstable. In the unstart regime, the thrust T in (1) is set to zero and simultaneously the coefficients of longitudinal force and moment are changed, as described in the following equations:

$$\begin{cases} \dot{V} = \dfrac{-D}{m} - g\sin\gamma \\ \dot{\gamma} = \dfrac{L}{mV} - \dfrac{g\cos\gamma}{V} \\ \dot{Q} = \dfrac{M_{yy}}{I_{yy}} \\ \dot{\vartheta} = Q \\ \dot{\alpha} = Q - \dfrac{L}{mV} + \dfrac{g\cos\gamma}{V} \end{cases}. \tag{7}$$

The state space equation is modified as follows:

$$\begin{cases} \dot{\boldsymbol{x}} = \boldsymbol{A}\boldsymbol{x} + \boldsymbol{B}\boldsymbol{\Lambda}(\boldsymbol{u} + \boldsymbol{f}(\boldsymbol{x})) \\ \boldsymbol{y} = \boldsymbol{C}\boldsymbol{x} \end{cases} \tag{8}$$

where $\boldsymbol{f}(\boldsymbol{x}) = \boldsymbol{\Theta}^{\mathrm{T}}\boldsymbol{\Phi}(\boldsymbol{x})$ represents uncertainty caused by inlet unstart; $\boldsymbol{\Theta} = [\theta_1\ \theta_2]^{\mathrm{T}}$ denotes the matrix of unknown constant parameters, $\boldsymbol{\Phi}(x)$ is the vector related to states, and $\boldsymbol{\Lambda}$ represents the change in elevator efficiency.

3. MRAC augmentation design of linear controller

3.1 Defining the reference model

The following equation is defined:

$$\boldsymbol{e}_y = \boldsymbol{y} - \boldsymbol{y}_{\mathrm{cmd}} \tag{9}$$

where $\boldsymbol{e}_y$ represents the system output tracking error, and $\boldsymbol{y}_{\mathrm{cmd}}$ indicates the command to be tracked. The integral of the output tracking error is defined as follows:

$$\dot{\boldsymbol{e}}_{yI} = \boldsymbol{e}_y = \boldsymbol{y} - \boldsymbol{y}_{\mathrm{cmd}} = \boldsymbol{C}\boldsymbol{x} - \boldsymbol{y}_{\mathrm{cmd}}. \tag{10}$$

Extending (8) with (10) produces the extended open-loop dynamic equations:

$$\begin{cases} \dot{\boldsymbol{x}}_{au} = \boldsymbol{A}_{au}\boldsymbol{x}_{au} + \boldsymbol{B}_{au}\boldsymbol{\Lambda}(\boldsymbol{u} + \boldsymbol{f}(x)) + \boldsymbol{B}_{\mathrm{ref}}\boldsymbol{y}_{\mathrm{cmd}} \\ \boldsymbol{y} = \boldsymbol{C}_{au}\boldsymbol{x}_{au} \end{cases} \tag{11}$$

where $\boldsymbol{x}_{au} = [\boldsymbol{e}_{yI}^{\mathrm{T}}\ \boldsymbol{x}^{\mathrm{T}}]^{\mathrm{T}}$ is the extended state vector. The extended open-loop matrices are as follows:

$$\boldsymbol{A}_{au} = \begin{bmatrix} \boldsymbol{0} & \boldsymbol{C} \\ \boldsymbol{0} & \boldsymbol{A} \end{bmatrix},$$

$$\boldsymbol{B}_{au} = \begin{bmatrix} \boldsymbol{0} \\ \boldsymbol{B} \end{bmatrix},$$

$$\boldsymbol{C}_{au}=\begin{bmatrix}\boldsymbol{0} & \boldsymbol{C}\end{bmatrix},$$
$$B_{\text{ref}}=\begin{bmatrix}-\boldsymbol{I}\\ \boldsymbol{0}\end{bmatrix}.$$

The assumption of $\boldsymbol{\Lambda}=\boldsymbol{I}$ and $\boldsymbol{f}(\boldsymbol{x})=\boldsymbol{0}$ in (11) results in the following linear baseline extended open-loop dynamic equations:

$$\begin{cases}\dot{\boldsymbol{x}}_{au}=\boldsymbol{A}_{au}\boldsymbol{x}_{au}+\boldsymbol{B}_{au}\boldsymbol{u}+\boldsymbol{B}_{\text{ref}}\boldsymbol{y}_{\text{cmd}}\\ \boldsymbol{y}=\boldsymbol{C}_{au}\boldsymbol{x}_{au}\end{cases}. \tag{12}$$

The baseline linear controller for baseline extended system (12) is designed in the following way.

The equation is defined as follows:

$$\begin{cases}\boldsymbol{z}=\dot{\boldsymbol{x}}_{au}=\begin{pmatrix}\dot{\boldsymbol{e}}_{yI}\\ \dot{\boldsymbol{x}}\end{pmatrix}\\ \boldsymbol{v}=\dot{\boldsymbol{u}}\end{cases}. \tag{13}$$

Then

$$\dot{\boldsymbol{z}}=\boldsymbol{A}_{au}\boldsymbol{z}+\boldsymbol{B}_{au}\boldsymbol{v}. \tag{14}$$

The linear quadratic cost index is as follows:

$$\boldsymbol{J}=\int_0^{\infty}\boldsymbol{z}^{\text{T}}\boldsymbol{Q}\boldsymbol{z}+\boldsymbol{v}^{\text{T}}\boldsymbol{R}\boldsymbol{v}\,\text{d}t \tag{15}$$

where $\boldsymbol{Q}$ and $\boldsymbol{R}$ are the appropriately selected symmetric positive-definite matrices. The corresponding optimal LQR solution is as follows:

$$\boldsymbol{v}=\dot{\boldsymbol{u}}=-\boldsymbol{R}^{-1}\boldsymbol{B}^{\text{T}}\boldsymbol{P}\boldsymbol{z}=-(\boldsymbol{K}_I\boldsymbol{K}_p)\begin{pmatrix}\dot{\boldsymbol{e}}_{yI}\\ \dot{\boldsymbol{x}}\end{pmatrix} \tag{16}$$

where $\boldsymbol{P}$ is the only symmetric positive-definite solution of the algebraic Riccati equation.

$$\boldsymbol{A}_{au}^{\text{T}}\boldsymbol{P}+\boldsymbol{P}\boldsymbol{A}_{au}+\boldsymbol{Q}-\boldsymbol{P}\boldsymbol{B}_{au}\boldsymbol{R}^{-1}\boldsymbol{B}_{au}^{\text{T}}\boldsymbol{P}=\boldsymbol{0}. \tag{17}$$

The following baseline linear controller is obtained by integrating (16)

$$\boldsymbol{u}_{bI}=-\boldsymbol{K}_{x_{au}}^{\text{T}}\boldsymbol{x}_{au}=-\boldsymbol{K}_I\boldsymbol{e}_{yI}-\boldsymbol{K}_p\boldsymbol{x}. \tag{18}$$

The block diagram of the baseline linear controller is shown in Fig. 1.

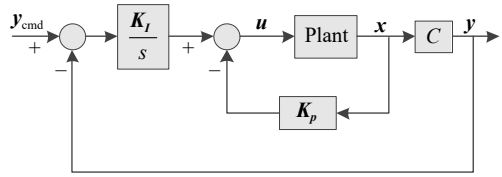

Fig. 1 Block diagram of baseline linear controller

Substituting (18) into (20) yields the following reference model dynamic equations:

$$\begin{cases}\dot{\boldsymbol{x}}_{\text{ref}}=\boldsymbol{A}_{\text{ref}}\boldsymbol{x}_{\text{ref}}+\boldsymbol{B}_{\text{ref}}\boldsymbol{y}_{\text{cmd}}\\ \boldsymbol{y}_{\text{ref}}=\boldsymbol{C}_{\text{ref}}\boldsymbol{x}_{\text{ref}}\end{cases} \tag{19}$$

where

$$\begin{cases}\boldsymbol{A}_{\text{ref}}=\boldsymbol{A}_{au}-\boldsymbol{B}_{au}\boldsymbol{K}_{x_{au}}^{\text{T}}\\ \boldsymbol{C}_{\text{ref}}=\boldsymbol{C}\end{cases}. \tag{20}$$

3.2 The design of MRAC

The presence of the uncertainties of the hypersonic vehicle may cause the tracking performance deterioration or even the instability of the baseline linear controller. In order to solve this problem and minimize the change of baseline linear controller, the controller should not only possess strong robustness to uncertainty, but also retain the advantages of simple form and easy engineering application of baseline linear control, therefore, an MRAC augmentation method of a linear controller is proposed. Thus, the total control input is the sum of baseline linear control and adaptive control [21].

$$\boldsymbol{u}=-\boldsymbol{K}_{x_{au}}^{\text{T}}\boldsymbol{x}_{au}+\boldsymbol{u}_{ad}=\boldsymbol{u}_{bI}+\boldsymbol{u}_{ad} \tag{21}$$

Substituting (21) into (11) and using (20) yield:

$$\begin{cases}\dot{\boldsymbol{x}}_{au}=\boldsymbol{A}_{\text{ref}}\boldsymbol{x}_{au}+\boldsymbol{B}_{au}\Lambda(\boldsymbol{u}_{ad}+(\boldsymbol{I}-\boldsymbol{\Lambda}^{-1})\boldsymbol{u}_{bI}+\boldsymbol{\Theta}^{\text{T}}\boldsymbol{\Phi}(x))+\boldsymbol{B}_{\text{ref}}\boldsymbol{y}_{\text{cmd}}\\ \boldsymbol{y}=\boldsymbol{C}_{\text{ref}}\boldsymbol{x}_{au}\end{cases}. \tag{22}$$

It is noted that

$$\boldsymbol{K}_u^{\text{T}}=\boldsymbol{I}-\boldsymbol{\Lambda}^{-1}. \tag{23}$$

Redefine vectors

$$\bar{\boldsymbol{\Phi}}(\boldsymbol{u}_{bI},\boldsymbol{x})=(\boldsymbol{u}_{bI}^{\text{T}}\ \boldsymbol{\Phi}^{\text{T}}(\boldsymbol{x}))^{\text{T}}. \tag{24}$$

Then the augmented matrix of unknown parameters is as follows:

$$\bar{\boldsymbol{\Theta}}=(\boldsymbol{K}_u^{\text{T}}\ \boldsymbol{\Theta}^{\text{T}})^{\text{T}}. \tag{25}$$

Then (22) can be rewritten as follows:

$$\begin{cases}\dot{\boldsymbol{x}}_{au}=\boldsymbol{A}_{\text{ref}}\boldsymbol{x}_{au}+\boldsymbol{B}_{au}\boldsymbol{\Lambda}(\boldsymbol{u}_{ad}+\bar{\boldsymbol{\Theta}}^{\text{T}}\bar{\boldsymbol{\Phi}}(\boldsymbol{u}_{bI},\boldsymbol{x}))+\boldsymbol{B}_{\text{ref}}\boldsymbol{y}_{\text{cmd}}\\ \boldsymbol{y}=\boldsymbol{C}_{\text{ref}}\boldsymbol{x}_{au}\end{cases} \tag{26}$$

The adaptive component $\boldsymbol{u}_{ad}$ is chosen to dominate the system uncertainty $\bar{\boldsymbol{\Theta}}^{\text{T}}\bar{\boldsymbol{\Phi}}(\boldsymbol{u}_{bI},\boldsymbol{x})$:

$$\boldsymbol{u}_{ad}=-\hat{\bar{\boldsymbol{\Theta}}}^{\text{T}}\bar{\boldsymbol{\Phi}}(\boldsymbol{u}_{bI},\boldsymbol{x}) \tag{27}$$

where $\hat{\bar{\boldsymbol{\Theta}}}$ is the matrix of adaptive parameters.

The state tracking error is as follows:

$$\boldsymbol{e}=\boldsymbol{x}_{au}-\boldsymbol{x}_{\text{ref}}. \tag{28}$$

Adaptive laws are selected in the following form:

$$\dot{\hat{\bar{\boldsymbol{\Theta}}}}=\boldsymbol{\Gamma}_{\bar{\Theta}}\bar{\boldsymbol{\Phi}}(\boldsymbol{u}_{bI},\boldsymbol{x})\boldsymbol{e}^{\text{T}}\boldsymbol{P}_{\text{ref}}\boldsymbol{B}_{au} \tag{29}$$

where elements $\boldsymbol{\Gamma}_{\bar{\Theta}}=\boldsymbol{\Gamma}_{\bar{\Theta}}^{\text{T}}>0$ represent adaptation rates and $\boldsymbol{P}_{\text{ref}}$ is the only symmetric positive-definite solution of the algebraic Lyapunov equation.

$$\boldsymbol{A}_{\text{ref}}^{\text{T}}\boldsymbol{P}_{\text{ref}}+\boldsymbol{P}_{\text{ref}}\boldsymbol{A}_{\text{ref}}=-\boldsymbol{Q}_{\text{ref}} \tag{30}$$

where $\boldsymbol{Q}_{\text{ref}}=\boldsymbol{Q}_{\text{ref}}^{\text{T}}>0$ is the appropriately chosen matrix.

The partitioning matrix $\boldsymbol{\Gamma}_{\bar{\theta}}$ is as follows:

$$\boldsymbol{\Gamma}_{\bar{\theta}}=\begin{pmatrix}\boldsymbol{\Gamma}_u & \boldsymbol{0}\\ \boldsymbol{0} & \boldsymbol{\Gamma}_{\theta}\end{pmatrix} \tag{31}$$

where $\boldsymbol{\Gamma}_u$ and $\boldsymbol{\Gamma}_{\theta}$ denote adaptation rates for uncertainties that correspond to $\boldsymbol{x}_{au}$ and $\boldsymbol{\Phi}(x)$. Equation (29) becomes as follows:

$$\begin{cases}\dot{\hat{\boldsymbol{K}}}_u=\boldsymbol{\Gamma}_u\boldsymbol{u}_{bI}\boldsymbol{e}^{\text{T}}\boldsymbol{P}_{\text{ref}}\boldsymbol{B}_{au}\\ \dot{\hat{\boldsymbol{\theta}}}=\boldsymbol{\Gamma}_{\theta}\boldsymbol{\Phi}(\boldsymbol{x})\boldsymbol{e}^{\text{T}}\boldsymbol{P}_{\text{ref}}\boldsymbol{B}_{au}\end{cases}. \tag{32}$$

The total control input is as follows:

$$\boldsymbol{u}=\boldsymbol{u}_{bl}+\boldsymbol{u}_{ad}=-\boldsymbol{K}_{x_{au}}^{\text{T}}\boldsymbol{x}_{au}-\hat{\boldsymbol{K}}_u^{\text{T}}\boldsymbol{u}_{bI}-\hat{\boldsymbol{\theta}}^{\text{T}}\boldsymbol{\Phi}(x). \tag{33}$$

The block diagram of adaptive augmentation of baseline linear controller is shown in Fig. 2. The adaptive gains $\hat{\boldsymbol{K}}_u$ and $\hat{\boldsymbol{\theta}}$ are driven by the tracking error $\boldsymbol{e}=\boldsymbol{x}_{au}-\boldsymbol{x}_{\text{ref}}$. Under the influence of adaptive augmentation of the reference linear controller, the output of system $\boldsymbol{y}$ tracks the output of reference model $\boldsymbol{y}_{\text{ref}}$ asymptotically in the presence of uncertainty $\boldsymbol{f}(\boldsymbol{x})=\boldsymbol{\Theta}^{\text{T}}\boldsymbol{\Phi}(\boldsymbol{x})$ and unknown elevator efficiency change $\boldsymbol{\Lambda}$ caused by inlet unstart.

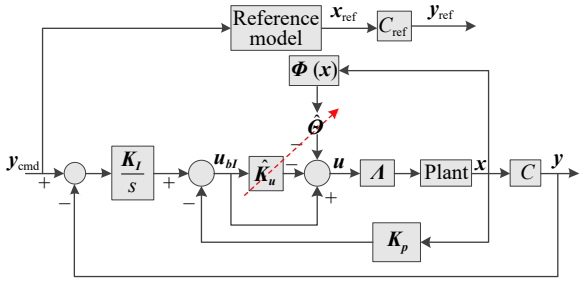

Fig. 2 Block diagram of adaptive augmentation of baseline linear controller

3.3 Demonstrating the stability of adaptive augmentation of the baseline linear controller

Equation (27) is substituted into (26):

$$\begin{cases}\dot{\boldsymbol{x}}_{au}=\boldsymbol{A}_{\text{ref}}\boldsymbol{x}_{au}-\boldsymbol{B}_{au}\boldsymbol{\Lambda}(\hat{\bar{\boldsymbol{\theta}}}-\bar{\boldsymbol{\theta}})^{\text{T}}\bar{\boldsymbol{\Phi}}+\boldsymbol{B}_{\text{ref}}\boldsymbol{y}_{\text{cmd}}\\ \boldsymbol{y}=\boldsymbol{C}_{\text{ref}}\boldsymbol{x}_{au}\end{cases} \tag{34}$$

where

$$\Delta\bar{\boldsymbol{\theta}}=\hat{\bar{\boldsymbol{\theta}}}-\bar{\boldsymbol{\theta}} \tag{35}$$

which is the matrix of parameter estimation error.

The tracking error dynamics is calculated by subtracting reference model (19) from the system (34):

$$\dot{\boldsymbol{e}}=\boldsymbol{A}_{\text{ref}}\boldsymbol{e}-\boldsymbol{B}_{au}\boldsymbol{\Lambda}\Delta\bar{\boldsymbol{\theta}}^{\text{T}}\bar{\boldsymbol{\Phi}}. \tag{36}$$

The following quadratic Lyapunov candidate function is selected:

$$V(\boldsymbol{e},\Delta\bar{\boldsymbol{\theta}})=\boldsymbol{e}^{\text{T}}\boldsymbol{P}_{\text{ref}}\boldsymbol{e}+\text{tr}(\Delta\bar{\boldsymbol{\theta}}^{\text{T}}\boldsymbol{\Gamma}_{\bar{\theta}}^{-1}\Delta\bar{\boldsymbol{\theta}}\boldsymbol{\Lambda}). \tag{37}$$

Equation (37) is differentiated as follows:

$$\dot{V}(\boldsymbol{e},\Delta\bar{\boldsymbol{\theta}})=-\boldsymbol{e}^{\text{T}}\boldsymbol{Q}_{\text{ref}}\boldsymbol{e}-2\boldsymbol{e}^{\text{T}}\boldsymbol{P}_{\text{ref}}\boldsymbol{B}_{au}\boldsymbol{\Lambda}\Delta\bar{\boldsymbol{\theta}}^{\text{T}}\bar{\boldsymbol{\Phi}}+2\text{tr}(\Delta\bar{\boldsymbol{\theta}}^{\text{T}}\boldsymbol{\Gamma}_{\bar{\theta}}^{-1}\dot{\hat{\bar{\boldsymbol{\theta}}}}\boldsymbol{\Lambda}). \tag{38}$$

If the following vector trace identity is applied to (38):

$$\boldsymbol{a}^{\text{T}}\boldsymbol{b}=\text{tr}(\boldsymbol{b}\boldsymbol{a}^{\text{T}}), \tag{39}$$

then the following equation is obtained:

$$\dot{V}(\boldsymbol{e},\Delta\bar{\boldsymbol{\theta}})=-\boldsymbol{e}^{\text{T}}\boldsymbol{Q}_{\text{ref}}\boldsymbol{e}+2\text{tr}\left(\Delta\bar{\boldsymbol{\theta}}^{\text{T}}\left\{\boldsymbol{\Gamma}_{\bar{\theta}}^{-1}\dot{\hat{\bar{\boldsymbol{\theta}}}}-\bar{\boldsymbol{\Phi}}\boldsymbol{e}^{\text{T}}\boldsymbol{P}_{\text{ref}}\boldsymbol{B}_{au}\right\}\boldsymbol{\Lambda}\right). \tag{40}$$

The substitution of (29) into (40) produces the following equation:

$$\dot{V}(\boldsymbol{e},\Delta\bar{\boldsymbol{\theta}})=-\boldsymbol{e}^{\text{T}}\boldsymbol{Q}_{\text{ref}}\boldsymbol{e}\leqslant 0. \tag{41}$$

The asymptotical stability of adaptive augmentation of baseline linear control is demonstrated with the Lyapunov stability theory.

3.4 Scheduling parameters of the RBF neural network

In Subsection 3.2, $\dot{\hat{\boldsymbol{K}}}_u$ represents the adaptive laws.

$$\dot{\hat{\boldsymbol{K}}}_u=\boldsymbol{\Gamma}_u\boldsymbol{u}_{bI}\boldsymbol{e}^{\text{T}}\boldsymbol{P}_{\text{ref}}\boldsymbol{B}_{au} \tag{42}$$

As we all know, the scheduling of adaptive control parameters is a very time-consuming work. In order to free designers from the cumbersome work and improve the work efficiency, this paper uses the approximation characteristics of the RBF neural network to design $\boldsymbol{\Gamma}_u$.

The RBF neural network uses a three-layer forward network. The input-to-output mapping is nonlinear, whereas the hidden-to-output layer mapping is linear, thereby greatly improving its learning speed and avoiding local minimum problem. The input signal uses system output tracking error $\boldsymbol{e}_y$ and its integration $\boldsymbol{e}_{yI}$. The hidden layer uses the Gaussian function as the base function. The output of the neural network is the parameters to be scheduled.

The structure of the neural network is shown in Fig. 3, and the 2-6-1 structure is adopted.

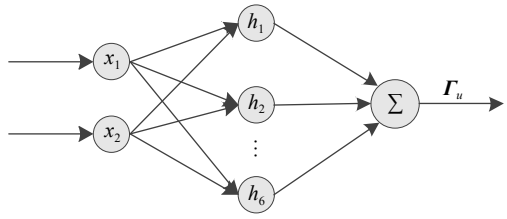

Fig. 3 Structure of RBF neural network

As shown in Fig. 3, $\boldsymbol{X}=[\boldsymbol{e}_{yI}\ \dot{\boldsymbol{e}}_{yI}]^{\text{T}}$ is selected as the input vector, the radial basis vector is defined as $\boldsymbol{H}=[h_1,$

$h_2,\cdots,h_i,\cdots,h_6]^{\mathrm{T}}$, where h_i is the Gaussian function.

$$h_i=\exp\left(-\frac{\|\boldsymbol{X}-\boldsymbol{C}_i\|^2}{2b_i^2}\right)\quad i=1,2,\cdots,6 \tag{43}$$

The center vector of the ith node of the neural network is

$$\boldsymbol{C}_i=[c_{i1}\ c_{i2}]^{\mathrm{T}}. \tag{44}$$

The base width vector of the neural network is assumed to be

$$\boldsymbol{B}=[b_1,b_2,\cdots,b_6]^{\mathrm{T}} \tag{45}$$

where b_i is the base width parameter of the node i, and satisfies $b_i>0$.

The weight vector of the neural network is

$$\boldsymbol{W}=[w_1,w_2,\cdots,w_6]^{\mathrm{T}}. \tag{46}$$

The output of the neural network $\boldsymbol{\Gamma}_u$ is

$$\boldsymbol{\Gamma}_u=\sum_{i=1}^{6}w_ih_i. \tag{47}$$

The performance index function is

$$J=\frac{1}{2}\dot{\boldsymbol{e}}_{\boldsymbol{yI}}^2=\frac{1}{2}(\boldsymbol{y}-\boldsymbol{y}_{\mathrm{cmd}})^2. \tag{48}$$

The base width parameter of the node, the value of the node center, and the output weight vector are calculated with the gradient descent method.

The base width parameter of the node is

$$\begin{aligned}\Delta b_i&=-\frac{\partial J}{\partial b_i}=-\dot{\boldsymbol{e}}_{\boldsymbol{yI}}\frac{\partial\dot{\boldsymbol{e}}_{\boldsymbol{yI}}}{\partial b_i}=-\dot{\boldsymbol{e}}_{\boldsymbol{yI}}\frac{\partial\boldsymbol{y}}{\partial b_i}=\\&-\dot{\boldsymbol{e}}_{\boldsymbol{yI}}\frac{\partial\boldsymbol{y}}{\partial\boldsymbol{\Gamma}_{\boldsymbol{u}}}\frac{\partial\boldsymbol{\Gamma}_{\boldsymbol{u}}}{\partial b_i}\approx-\dot{\boldsymbol{e}}_{\boldsymbol{yI}}\frac{\partial\boldsymbol{\Gamma}_{\boldsymbol{u}}}{\partial b_i}=\\&-\dot{\boldsymbol{e}}_{\boldsymbol{yI}}w_ih_i\frac{\|\boldsymbol{X}-\boldsymbol{C}_i\|^2}{b_i^3}.\end{aligned} \tag{49}$$

$$b_i(k)=b_i(k-1)+\eta\Delta b_i+\mu(b_i(k-1)-b_i(k-2)) \tag{50}$$

The value of the node center is

$$\begin{aligned}\Delta c_{ij}&=-\frac{\partial J}{\partial c_{ij}}=-\dot{\boldsymbol{e}}_{\boldsymbol{yI}}\frac{\partial\dot{\boldsymbol{e}}_{\boldsymbol{yI}}}{\partial c_{ij}}=-\dot{\boldsymbol{e}}_{\boldsymbol{yI}}\frac{\partial\boldsymbol{y}}{\partial c_{ij}}=\\&-\dot{\boldsymbol{e}}_{\boldsymbol{yI}}\frac{\partial\boldsymbol{y}}{\partial\boldsymbol{\Gamma}_{\boldsymbol{u}}}\frac{\partial\boldsymbol{\Gamma}_{\boldsymbol{u}}}{\partial c_{ij}}\approx-\dot{\boldsymbol{e}}_{\boldsymbol{yI}}\frac{\partial\boldsymbol{\Gamma}_{\boldsymbol{u}}}{\partial c_{ij}}=\\&-\dot{\boldsymbol{e}}_{\boldsymbol{yI}}w_ih_i\frac{X_i-c_{ij}}{b_i^2}.\end{aligned} \tag{51}$$

$$c_{ij}(k)=c_{ij}(k-1)+\eta\Delta c_{ij}+\mu(c_{ij}(k-1)-c_{ij}(k-2)) \tag{52}$$

where j=1, 2.

The output weight vector is

$$\begin{aligned}\Delta w_i&=-\frac{\partial J}{\partial w_i}=-\dot{\boldsymbol{e}}_{\boldsymbol{yI}}\frac{\partial\dot{\boldsymbol{e}}_{\boldsymbol{yI}}}{\partial w_i}=-\dot{\boldsymbol{e}}_{\boldsymbol{yI}}\frac{\partial\boldsymbol{y}}{\partial w_i}=\\&-\dot{\boldsymbol{e}}_{\boldsymbol{yI}}\frac{\partial\boldsymbol{y}}{\partial\boldsymbol{\Gamma}_{\boldsymbol{u}}}\frac{\partial\boldsymbol{\Gamma}_{\boldsymbol{u}}}{\partial w_i}\approx-\dot{\boldsymbol{e}}_{\boldsymbol{yI}}\frac{\partial\boldsymbol{\Gamma}_{\boldsymbol{u}}}{\partial w_i}=-\dot{\boldsymbol{e}}_{\boldsymbol{yI}}h_i.\end{aligned} \tag{53}$$

$$w_i(k)=w_i(k-1)+\eta\Delta w_i+\mu(w_i(k-1)-w_i(k-2)) \tag{54}$$

where η is the learning speed, μ is the learning factor, $0<\eta<1$, and $0<\mu<1$.

4. Simulation results and analysis

The MRAC augmentation method of a baseline linear controller is simulated and applied to an AHV to verify its effectiveness.

The assumed simulation conditions are listed in Table 1. A commanded angle of attack is tracked. In the beginning, the inlet is started, and the baseline linear controller is designed for the baseline extended system. When the angle of attack reaches 10°, the inlet unstarts, and the model perturbs on the basis of the baseline model. The perturbation is as follows: $\boldsymbol{\Theta}=[\theta_1\ \theta_2]^{\mathrm{T}}=[0.025a_2-0.025a_1]^{\mathrm{T}}$, $\boldsymbol{\Phi}(x)=[\alpha\ Q]^{\mathrm{T}}$, $\boldsymbol{\Lambda}=0.6$. That is to say, the absolute value of the kinetic coefficient a_2 increases by 45%, a_3 and a_5 decrease by 40%, a_4 decreases by 6%, and a_1 decreases by 45%.

Table 1 Simulation conditions

Symbol	Description	Value
H_0/km	Initial height	23
Ma_0	Initial Ma number	6
α_0/(°)	Initial angle of attack	2.5
Q_0/(°·s^{-1})	Initial pitch rate	0

Thereafter, two control methods are adopted, one is the baseline linear control method, and the other is the MRAC augmentation method. When the angle of attack is stabilized to −5°, the inlet restarts. The simulation results of the two methods are compared and shown in Fig. 4−Fig. 8.

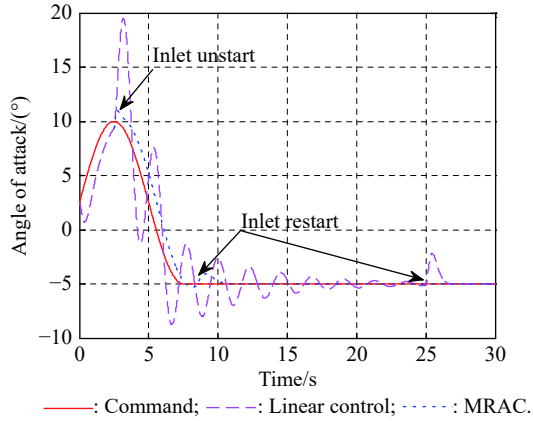

Fig. 4 Time histories of angle of attack

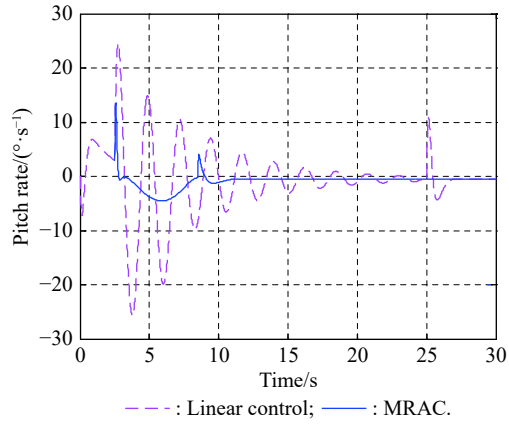

Fig. 5 Time histories of the pitch rate

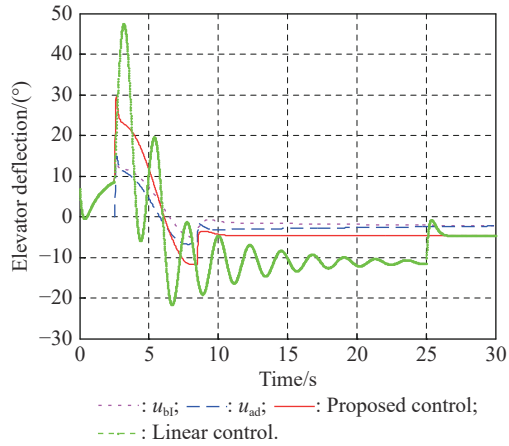

Fig. 6 Time histories of elevator deflection angle

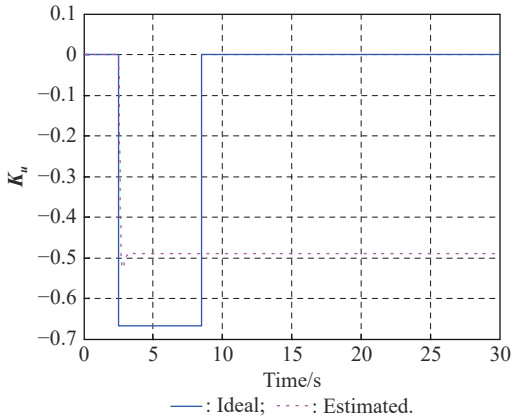

Fig. 7 Time histories of the parameter K_u

As shown in Fig. 4–Fig. 6, in the beginning, the baseline linear control method has a good control performance for the baseline model, and the output of the system can track its command well. Pitch rate is less than 10°/s and maximum elevator deflection angle is 9.8°.

When the inlet unstart, the pitch rate, elevator deflection angle, and angle of attack controlled by the baseline linear control method have a sustained large oscillation, and the maximum amplitude reaches about 25°/s, 38°, and 11° respectively. At 25 s, the angle of attack stabilizes to −5° and the inlet restarts. The pitch rate controlled by the MRAC augmentation method remains stable after a small oscillation. The elevator deflection angle changes obviously, and the amplitude reaches about 20°, then it converges rapidly. The angle of attack only produces a perturbation of 1°, and after 0.2 s it begins to track the angle of attack command. At 8.5 s, the angle of attack stabilizes to −5°, and the inlet restarts. The MRAC augmentation method is superior than the linear control method in the unstart regime.

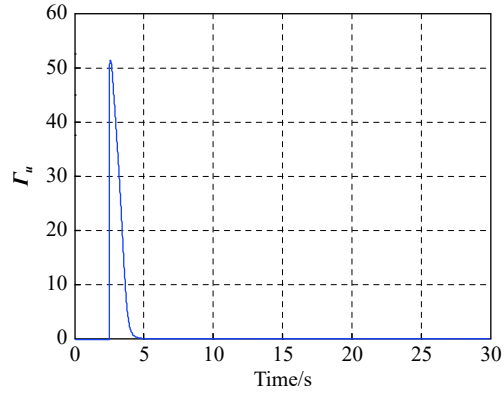

Fig. 8 Time histories of the adaptive rate Γ_u

After the inlet restart, the control performances of the two methods are similar, and both methods have good control effect on the vehicle with started inlet.

In Fig. 6, the red solid line denotes the total control input, the dot line represents the elevator deflection angle generated by the linear control method, and the dash line is the elevator deflection angle generated by the adaptive control method. When the MRAC augmentation method of linear controller is adopted from 2.5 s, the total control input is the sum of the elevator deflection angle generated by the adaptive control and the elevator deflection angle generated by the linear control.

The estimated values of parameter $\boldsymbol{K}_u$ converge, as shown in Fig. 7. Fig. 8 shows the adaptive rate $\boldsymbol{\Gamma}_u$ scheduled by the RBF neural network.

In order to prove the superiority of the proposed method, it is compared with the conventional MRAC. The simulation results are shown in Fig. 9–Fig. 11. It can be seen from the figure that after the inlet unstart, the maximum values of oscillation process of angle of attack, pitch rate and elevator deflection angle controlled by the conventional MRAC method reach 11.5°, 22.5°/s and 38.5°, respectively, which are larger than 11.0°, 13.4°/s, 29.6° controlled by the proposed method. It proves that the oscillation process controlled by the proposed method has smaller amplitude and faster convergence than the conventional MRAC method.

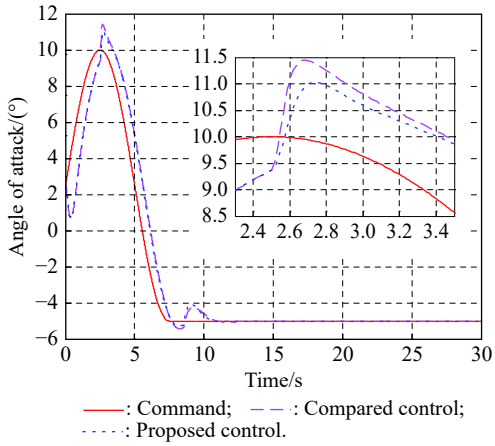

Fig. 9 Angle of attack controlled by both methods

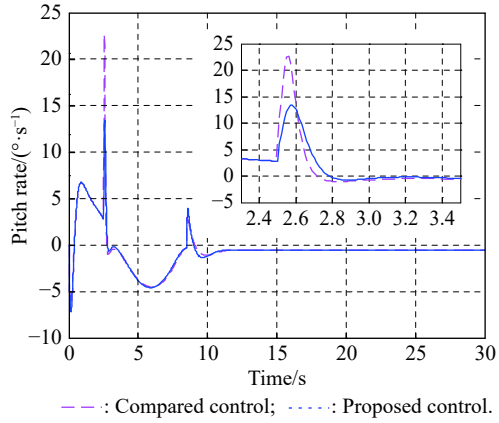

Fig. 10 Pitch rate controlled by both methods

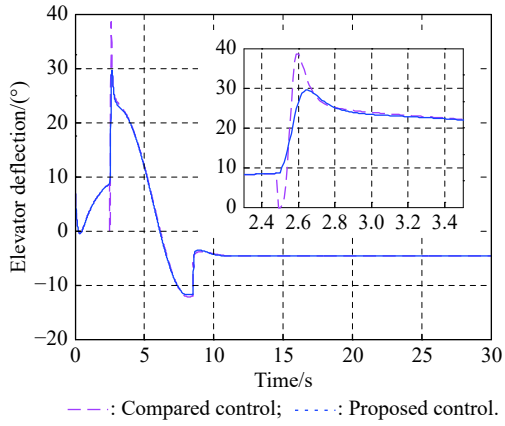

Fig. 11 Eevator deflection angle controlled by both methods

The simulation results show that the MRAC augmentation method of a linear controller is strongly adaptive and robust to parameter changes caused by inlet unstart. The proposed method can stabilize the attitude of the hypersonic vehicle more quickly than the linear control method after the inlet unstart, which provides favorable conditions for inlet restart. Compared with the conventional MRAC, the amplitude of the oscillation process controlled by the proposed method is smaller and the convergence is faster.

In terms of computational complexity, the proposed method mainly increases the calculations of the baseline controller and RBF neural network compared with the traditional MRAC. These two parts only need basic calculations, and there is no need for other time-consuming calculations such as optimization and iteration. Therefore, the proposed method is equivalent to the traditional MRAC in terms of computational complexity, which has no obvious increase in complexity.

5. Conclusions

The inlet unstart control problem is a very interesting and challenging work. This paper establishes the model of AHV after inlet unstart to describe the changes of flight dynamics caused by inlet unstart of scramjet. Based on this model, an MRAC augmentation method of a linear controller is proposed. The method can stabilize the attitude of the AHV quickly after inlet unstart and provide favorable conditions for the inlet restart. The main superiority of the proposed method over linear control and conventional MRAC is the improvement of the dynamic performance of the control system after inlet unstart. The integration of RBF neural network to schedule parameters of the adaptive controller further simplifies the design process and enhances the efficiency of parameter scheduling.

References

[1] BROCANELLI M, GUNBATAR Y, SERRANI A, et al. Robust control for unstart recovery in hypersonic vehicles. Proc. of the AIAA Guidance, Navigation, and Control Conference, 2012: 1–20.

[2] WALKER S, RODGERS F, PAULL A, et al. HyCAUSE flight test program. Proc. of the 15th AIAA International Space Planes and Hypersonic Systems and Technologies Conference, 2008: 1–14.

[3] LEWIS M. X-51 scrams into the future. Aerospace America, 2010, 48(9): 27–31.

[4] MUSIELAK D. High-speed air-breathing propulsion. Aerospace America, 2011, 49(11): 49.

[5] IM S, DO H. Unstart phenomena induced by flow choking in scramjet inlet-isolators. Progress in Aerospace Sciences, 2018, 97: 1–21.

[6] KONG C, CHANG J T, LI Y F, et al. Flowfield reconstruction and shock train leading edge detection in scramjet isolators. AIAA Journal, 2020, 58(9): 4068–4080.

[7] DEVARAJ M K K, JUTUR P, RAO S M V, et al. Experimental investigation of unstart dynamics driven by subsonic spillage in a hypersonic scramjet intake at Mach 6. Physics of Fluids, 2020, 32(2): 026103.

[8] XUE L S, WANG C P, CHENG K M, et al. Dynamic characteristics of separation shock in an unstarted hypersonic inlet flow. AIAA Journal, 2018, 56(6): 2484–2490.

[9] LI N, CHANG J T, JIANG C Z, et al. Unstart/restart hyster-

esis characteristics analysis of an over-under TBCC inlet caused by backpressure and splitter. Aerospace Science and Technology, 2017, 72: 418–425.
[10] DENG R Y, JIN Y Z, KIM H D, et al. Numerical simulation of the unstart process of dual-mode scramjet. International Journal of Heat and Mass Transfer, 2017, 105: 394–400.
[11] BOLENDER M A, WILKIN H, JACOBSEN L, et al. Flight dynamics of a hypersonic vehicle during inlet un-start. Proc. of the 16th AIAA/DLR/DGLR International Space Planes and Hypersonic System and Technologies Conference, 2009. DOI: 10.2514/6.2009-7292.
[12] WIESE D P, ANNASWAMY A M, MUSE J A, et al. Adaptive control of a generic hypersonic vehicle. Proc. of the AIAA Guidance, Navigation, and Control Conference, 2013. DOI: https://doi.org/10.2514/6.2013-4514.
[13] LAVRETSKY E, GADIENT R, GREGORY I M. Predictor-based model reference adaptive control. Journal of Guidance, Control and Dynamics, 2010, 33(4): 1195–1201.
[14] LAVRETSKY E, HOVAKIMYAN N. Stable adaptation in the presence of actuator constraints with flight control applications. Journal of Guidance, Control and Dynamics, 2007, 30(2): 337–345.
[15] HASSOUN M H. Fundamentals of artificial neural networks. Cambridge: MIT Press, 1995.
[16] WANG J M, WANG J B, ZHANG T. RBF neural network based adaptive sliding mode control for hypersonic flight vehicles. Proc. of the IEEE Chinese Guidance, Navigation and Control Conference, 2016: 58–63.
[17] ZHAI R Y, QI R Y, JIANG B. Adaptive sliding mode fault-tolerant control for hypersonic aircraft using RBF neural networks. Proc. of the Chinese Control and Decision Conference, China, 2016: 1879–1884.
[18] SLAMA S, ERRACHDI A, BENREJEB M. Model reference adaptive control for MIMO nonlinear systems using RBF neural networks. Proc. of the International Conference on Advanced Systems and Electric Technologies, 2018: 346–351.
[19] BOLENDER M A, DOMAN D B. Nonlinear longitudinal dynamical model of an air-breathing hypersonic vehicle. Journal of Spacecraft and Rockets, 2007, 44(2): 374–387.
[20] PARKER J T, SERRANI A, YURKOVICH S, et al. Control-oriented modeling of an air-breathing hypersonic vehicle. Journal of Guidance, Control and Dynamics, 2007, 30(3): 856–869.
[21] LAVRETSKY E, WISE K A. Robust and adaptive control with aerospace applications. New York: Springer Verlag, 2013.

Biographies

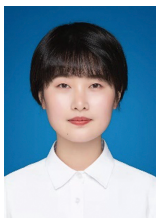

WANG Fan was born in 1991. She received her B.S. and M.S. degrees in guidance, navigation, and control from the School of Astronautics, Northwestern Polytechnical University, Xi'an, Shaanxi Province, China, in 2014 and 2017. She is a Ph.D. candidate with the School of Astronautics, Northwestern Polytechnical University. Her research interests include hypersonic vehicle control, nonlinear control, and adaptive control.
E-mail: wangf@mail.nwpu.edu.cn

FAN Pengfei was born in 1987. He received his B.S., M.S., and Ph.D. degrees in guidance, navigation and control from the School of Astronautics, Northwestern Polytechnical University, Xi'an, Shaanxi Province, China, in 2010, 2013 and 2020, respectively. Since 2020, he has been an assistant researcher at School of Astronautics, Northwestern Polytechnical University. His research interests are trajectory optimization and three-dimensional guidance technology for entry vehicle.
E-mail: fanpf@mail.nwpu.edu.cn

FAN Yonghua was born in 1976. He received his B.S. degree in mechanics and control from the Second Artillery Engineering University, Xi'an, Shaanxi Province, China, in 1998 and his Ph.D. degree in control theory and engineering from Northwestern Polytechnical University, Xi'an, Shaanxi Province, China, in 2008. Now he is a professor at School of Astronautics, Northwestern Polytechnical University. His research interests are guidance and control for UAV.
E-mail: fyhlixin@163.com

XU Bin was born in 1982. He received his B.S. degree in measurement and control from Northwestern Polytechnical University, Xi'an, Shaanxi Province, China, in 2006 and the Ph.D. degree in computer science from Tsinghua University, Beijing, China, in 2012. He visited Swiss Federal Institute of Technology in Zurich from March 2010 to March 2011. He was a research fellow with Nanyang Technological University from February 2012 to January 2013. He has been with the School of Automation, Northwestern Polytechnical University as a lecturer from July 2012 to April 2014. Now he is a professor at the School of Automation, Northwestern Polytechnical University. His research interests are intelligent control and adaptive control with application on flight dynamics.
E-mail: binxu@nwpu.edu.cn

YAN Jie was born in 1960. He received his Ph.D. degree from School of Astronautics, Northwestern Polytechnical University Xi'an, Shaanxi Province, China, in 1988. He is currently working as a professor and Ph.D. candidate supervisor at the School of Astronautics, Northwestern Polytechnical University. His research interests are flight control, guidance, system simulation and aircraft design.
E-mail: jyan@nwpu.edu.cn